



**Twist dynamics and buckling instability of ring DNA: the effect of groove asymmetry and anisotropic bending**

Journal:	<i>Soft Matter</i>
Manuscript ID	SM-ART-10-2020-001812.R2
Article Type:	Paper
Date Submitted by the Author:	03-Dec-2020
Complete List of Authors:	Gutierrez Fosado, Yair Augusto; Aoyama Gakuin University - Sagamihara Campus, Department of Physics and Mathematics Landuzzi, Fabio; Aoyama Gakuin University - Sagamihara Campus, Department of Physics and Mathematics Sakaue, Takahiro; Aoyama Gakuin University College of Science and Engineering Graduate School of Science and Engineering, Department of Physics and Mathematics

Cite this: DOI: 00.0000/xxxxxxxxxx

## Twist dynamics and buckling instability of ring DNA: the effect of groove asymmetry and anisotropic bending<sup>†</sup>

Yair Augusto Gutiérrez Fosado,<sup>‡a</sup> Fabio Landuzzi,<sup>‡a</sup> and Takahiro Sakaue<sup>\*ab</sup>

Received Date

Accepted Date

DOI: 00.0000/xxxxxxxxxx

By combining analytical theory and Molecular Dynamics simulations we study the relaxation dynamics of DNA circular plasmids that initially undergo a local twist perturbation. In this process, the twist-bend coupling arising from the groove asymmetry in the DNA double helix clearly manifests. In the two scenarios explored, with/without this coupling, the initial perturbation relaxes diffusively. However, there are some marked differences on the value of the diffusion coefficient and the dynamics in both cases. These differences can be explained by assuming the existence of three distinctive time scales; (*I*) a rapid relaxation of local bending, (*II*) the slow twist spreading, and (*III*) the buckling transition taking place in a much longer time scale. In particular, the separation of time scales allows to deduce an effective diffusion equation in stage (*II*), with a diffusion coefficient influenced by the twist-bend coupling. We also discuss the mapping of the realistic DNA model to the simpler isotropic twistable worm-like chain using the renormalized bending and twist moduli; although useful in many cases, it fails to make a quantitative prediction on the instability mode of buckling transition.

### 1 Introduction

It has become increasingly evident that not only the genetic information encoded in the DNA is relevant in several biological processes, but also that the elastic properties of DNA and its topology play a key role in its functioning<sup>1–3</sup>. In the transcription process, for example, the RNA polymerase locally reshapes DNA as it reads the sequence along it. This local deformation generates stress of the helix that dynamically drives overtwisting ahead and undertwisting behind the polymerase<sup>4</sup>. It has been hypothesized that this stress could influence the dynamics of nucleosomes, the binding of proteins along the DNA, the gene expression, among other regulatory processes<sup>5–7</sup>. Thus changing the role we perceive DNA from a passive entity that storage information to an active participant of the regulation of gene activity.

To address the elastic response of DNA to mechanical manipulations, the isotropic twistable worm-like-chain (TWLC) model is usually employed. This model describes double-stranded (ds) DNA as an inextensible and isotropic elastic rod characterized by only two elastic constants: the bending stiffness ( $A$ ) and the tor-

sional stiffness ( $C$ ). However, the actual DNA is equipped with hard and soft directions for bending (anisotropy), and furthermore, the geometrical asymmetry imposed by the presence of the minor and major grooves of the dsDNA helix gives rise to a coupling between twist and bend<sup>8</sup>. Recent studies have revealed that these elements, not included in the isotropic TWLC, are relevant to the DNA physics in several contexts, including the bending and twisting of DNA in the nucleosome scale<sup>9–11</sup>.

Despite its importance, the study in this direction has so far been restricted to the equilibrium dynamics, which thus does not resolve important time-dependent processes, such as how efficiently torsional stress is transported to distal DNA sites. Here we try to shed some light onto this subject by combining an analytical theory and Molecular Dynamic (MD) simulations. The protocol we employ in this study is depicted in Figure 1: initially, a segment of the DNA ( $l$  out of total  $N$  base pairs) is constrained to have a twist density deficit  $\Omega_3 = \Delta\chi_p$  (blue line in the plot). After the constraint is released at  $t = 0$ , the system relaxes (yellow line) to a state of uniform twist deficit  $\Omega_3 = \Delta\chi_p l/N$  (purple line in the plot) that is reached after a time  $t^*$ . For  $t \gg t^*$  the buckling of the molecule is observed as the twist density tends (cyan line) to its relaxed state  $\Omega_3 = 0$ . This protocol allows us to investigate the rate at which the stress can be relieved through the propagation of an over/under twisted region of a short DNA ring to the adjacent base-pairs.

<sup>a</sup> Department of Physics and Mathematics, Aoyama Gakuin University 5-10-1 Fuchinobe, Chuo-ku, Sagami-hara-shi, Kanagawa 252-5258, Japan.

<sup>b</sup> PRESTO, Japan Science and Technology Agency (JST), 4-1-8 Honcho Kawaguchi, Saitama 332-0012, Japan.

<sup>†</sup> Electronic Supplementary Information (ESI) available: Document with details of the simulations and the theory described in the main text and two movies are provided. See DOI: 10.1039/cXsm00000x/

<sup>‡</sup> Joint first authors.

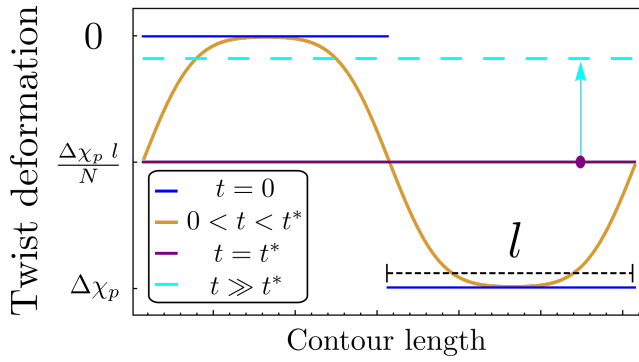


**Fig. 1** Schematic representation of the protocol we employed to measure the diffusion of twist. Different colors represent the local-twist at different times.

## 2 Reminder on the model

Let us describe the center line of the DNA as a curve,  $r(s)$ , parameterized by arc length ( $s$ ) and with a fixed total length  $L$ . Its conformation is completely characterized by the set of orthonormal vectors  $\{\hat{e}_1(s), \hat{e}_2(s), \hat{e}_3(s)\}$  that define a local reference frame (the Darboux frame) at each point  $s$  on the curve. The tangent vector to the center line is  $\hat{e}_3 = \frac{d}{ds}r(s)$  and by convention,  $\hat{e}_1$  lies in the symmetry axis of the grooves in the direction of the major groove and  $\hat{e}_2 = \hat{e}_3 \times \hat{e}_1$  (see Fig 2). Associated with the conformation, there is a local strain  $\Omega(s) = \Omega_1(s)\hat{e}_1(s) + \Omega_2(s)\hat{e}_2(s) + \Omega_3(s)\hat{e}_3(s)$ , that connects two reference frames located at  $s$  and  $s + ds$ . This satisfies

$$\frac{d\hat{e}_i}{ds} = [\Omega + \chi_0\hat{e}_3(s)] \times \hat{e}_i(s), \quad (1)$$

with  $i = 1, 2, 3$  and  $\chi_0 (\simeq 1.75 \text{ nm}^{-1})$  the intrinsic twist density of the DNA helix. The three components of the deformation vector are  $\Omega_i(s) = \Omega(s) \cdot \hat{e}_i(s)$ , where  $\Omega_3$  is the local excess (or deficit) of twist density with respect to  $\chi_0$ , and,  $\Omega_1$  and  $\Omega_2$  represent the bending densities related to the tilt and roll degrees of freedom of the dsDNA.

The elastic free energy functional in terms of the local deformations truncated at quadratic order is  $E = \int_0^L \varepsilon_0(\Omega) ds$ <sup>8</sup>, with

$$\begin{aligned} \varepsilon_0(\Omega) &= \frac{1}{2}(A_1\Omega_1^2 + A_2\Omega_2^2 + C\Omega_3^2 + 2G\Omega_2\Omega_3) \\ &= \frac{A_1}{2}\Omega_1^2 + \frac{A_2}{2}\left(\Omega_2 + \frac{G}{A_2}\Omega_3\right)^2 + \frac{\tilde{C}}{2}\Omega_3^2, \end{aligned} \quad (2)$$

where the bending rigidities about the axes  $\hat{e}_1$  and  $\hat{e}_2$  are  $A_1$  and  $A_2$ , respectively.  $C$  expresses the torsional stiffness and  $G$  represents the twist-bend coupling between the local deformations  $\Omega_2$  and  $\Omega_3$ . These parameters, in general, depend on the sequence of the molecule<sup>12</sup> and therefore on  $s$ , but for simplicity here we only consider a homopolymer (made of only GC pairs) for which they are constant<sup>12</sup>. Important features of the model become transparent if the energy density is transformed into a complete square as in the second equality of Eq. (2), where  $\tilde{C} = C\left(1 - \frac{G^2}{A_2C}\right)$  is the renormalized twist modulus. The consequence of this

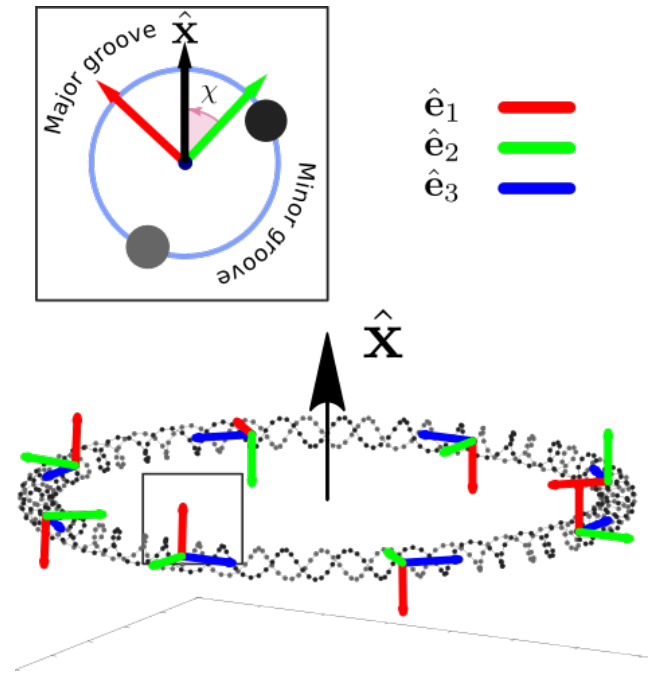


**Fig. 2** Schematic representation of a DNA ring. The vector  $\hat{x}$  points in the perpendicular direction to the plane spanned by the ring. The position of the phosphates is depicted in black and gray for the two DNA strands. At each base-pair an orthonormal frame is defined:  $\hat{e}_3$  is the tangent to the helix axis, while  $\hat{e}_1$  and  $\hat{e}_2$  lie on the plane of the Watson-Crick bases. To ease the visualization we only show reference frames at eight different positions (approximately every 3.75 helical turns). A cross section of the helix is shown in the top panel. For configurations close to the planar circle, the plane formed by  $\hat{e}_1$  and  $\hat{e}_2$  contains the vector  $\hat{x}$ . The angle between  $\hat{e}_2$  and  $\hat{x}$  is  $\chi$ .

renormalization is evident after integrating out the bending degrees of freedom from the weight  $P(\{\Omega_i\}) \propto e^{-\beta\varepsilon_0(\{\Omega_i\})}$  (see ESI †), implying the softening of twisting response. Similarly, the bending about  $\hat{e}_2$  is affected with a renormalized modulus  $\tilde{A}_2 = A_2\left(1 - \frac{G^2}{A_2C}\right)$ .

The bending ( $l_b$ ) and torsional ( $l_\tau$ ) persistence lengths that are usually defined by the correlation of the reference frames along  $s$ , can be expressed in terms of these renormalized elastic constants<sup>13</sup>:  $l_b = \beta\tilde{A}$  and  $l_\tau = 2\beta\tilde{C}$  where  $\tilde{A} = \frac{2}{A_1^{-1} + \tilde{A}_2^{-1}}$  is the harmonic mean of  $A_1$  and  $\tilde{A}_2$ .

### 2.1 Closed configurations

The elastic free energy functional in terms of the local deformations has been thoroughly studied in the past for linear<sup>8,12</sup> and ring<sup>9,10</sup> molecules. Following reference<sup>10</sup>, here we employ the energy density  $\varepsilon$  for a torsionally constraint DNA ring

$$\varepsilon(\Omega) = \varepsilon_0(\Omega) - \mu[\Omega_1 \sin(\chi s) + \Omega_2 \cos(\chi s)] - \lambda\Omega_3, \quad (3)$$

where the last two terms with Lagrange multipliers  $\mu$  and  $\lambda$  represent the ring closure constraint, which allows to analytically describe the minimum energy configuration of a ring<sup>10</sup>. The first term enforces the bending ( $\Omega_b = \Omega_1 + \Omega_2$ ) to take place along the unitary vector  $\hat{x} = \sin(\chi s)\hat{e}_1 + \cos(\chi s)\hat{e}_2$  pointing in the di-

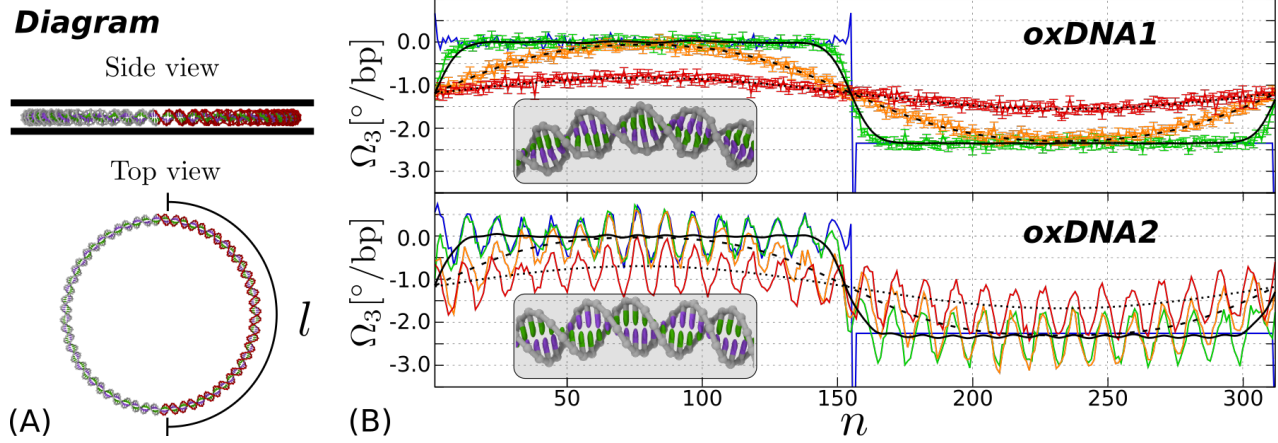


**Fig. 3** Twist diffusion. **(A)** Sketch of the system. A ring DNA molecule is confined in between two parallel planes (results for simulations without the planes are also discussed in the main text). The region with the  $\Delta Lk = -1$  deficit ( $l = 156$  out of  $N = 312$  base-pairs) is highlighted in red. **(B)** Local twist deformation  $\Omega_3$  as function of the contour length for oxDNA1 (top) and oxDNA2 (bottom). Color lines (blue, green, yellow and red) represent results at different times ( $t = 0, 5, 2500$  and  $15000\tau_L$ ). Black lines (solid, dashed and dotted) are solutions to the diffusion equation at the corresponding times for  $t > 0$  (see ESI† for details). The insets show sections in the relaxed part of the ring before the release of under-twist.

rection perpendicular to the plane spanned by the molecule (see Fig. 2), while the second term accounts for the presence of twist excess  $\Delta\chi = \chi - \chi_0$ .

Notably, the renormalized elastic constants enter in the equations that identify the ground state of ring DNA molecules. This is found by the minimization of the energy density with respect to  $\Omega_i$ . Thus, the elastic strains at ground state for a torsionally stressed planar ring are

$$\begin{aligned}\Omega_1^0(s) &= \frac{\mu}{A_1} \sin(\chi s), \\ \Omega_2^0(s) &= \frac{\mu}{\tilde{A}_2} \cos(\chi s) - \frac{\lambda G}{\tilde{C} \tilde{A}_2}, \\ \Omega_3^0(s) &= -\frac{\mu G}{C \tilde{A}_2} \cos(\chi s) + \frac{\lambda}{\tilde{C}}.\end{aligned}\quad (4)$$

where  $\mu = k_B T l_b / R_0$  is identified with the external bending torque enforcing a radius  $R_0$  on a ring with a bending persistence length  $l_b$ <sup>9</sup>, while  $\lambda = \tilde{C} \Delta\chi$  is the external twisting torque as inspected from the relation  $\int_0^L ds \Omega_3^0(s) (= \Delta\chi L) = \lambda L / \tilde{C}$ . The oscillation of  $\Omega_1^0$  and  $\Omega_2^0$  is a natural consequence of the DNA helical structure. Marked features here are: (i) the anisotropy ( $A_1 \neq \tilde{A}_2$ ) implies unequal bending amplitudes, leading to the non-constant curvature  $\kappa(s) = \sqrt{(\Omega_1^0(s))^2 + (\Omega_2^0(s))^2}$ ; (ii) the twist-bend coupling ( $G > 0$ ) induces a “twist wave”, i.e., a periodic modulation in  $\Omega_3^0(s)$  which is in anti-phase with  $\Omega_2^0(s)$ ; and (iii) it produces a constant shift in  $\Omega_2^0(s)$  and  $\Omega_3^0(s)$ . It is also worth mentioning that the ground state energy

$$\oint ds \varepsilon(\Omega_1^0(s), \Omega_2^0(s), \Omega_3^0(s)) = \left( \frac{1}{2} \frac{\tilde{A}}{R_0^2} + \frac{1}{2} \tilde{C} (\delta\chi)^2 \right), \quad (5)$$

is formally identical to that of the isotropic TWLC ring (with constant radius of curvature  $R_0$ ) with bending and twist moduli  $\tilde{A}$  and  $\tilde{C}$ , respectively. Although at first sight it is not obvious how

the nontrivial structural properties discussed here affect the twist dynamics in real DNA, in the following we attempt to get some insight into this.

## 3 Results and discussion

### 3.1 Coarse-grained simulations of DNA

Here we study the dynamics of twist in the oxDNA<sup>14,15</sup>, a coarse-grained model that is based on force fields tuned to account for several geometrical and thermodynamic features of single and double stranded DNA (in its B form). One important feature of the oxDNA model for the current study is that two parameterizations are available, namely, oxDNA1 and oxDNA2. While the former describes dsDNA as a molecule with symmetric grooves, the latter introduces the appropriate groove asymmetry found in real DNA. Therefore, as it has already been shown, there is a direct mapping between these models and the theory described in the previous section<sup>9,10,12</sup>. The oxDNA1 resembles the anisotropic TWLC model ( $G = 0, C > 0$  and  $A_1 \neq A_2$ ) and the oxDNA2 the more general case in which all the stiffness parameters play a role in the description.

We first investigate the diffusion of twist by performing coarse-grained molecular dynamics simulations of dsDNA rings with a total length of  $N = 312$  bp. The protocol we follow is described in ESI † and it is similar to that on<sup>16</sup>. Briefly, the molecule is initialized with the mean distance between successive base-pairs  $a = 0.34$  nm. The local twist in half of the ring is set to its natural value:  $a\chi_0 = 34.5^\circ$  and  $34.1^\circ$  for oxDNA1 and oxDNA2, hence  $\Omega_3(s, t = 0) = 0$  for  $s \in [1, l]$ , with  $l = N/2$ . In the other half, a deficit (or excess) of one helical turn is introduced such that  $\Delta\chi_p \equiv \Omega_3(s, t = 0) = -2\pi/la$  for  $s \in (l, N]$ . Importantly these conditions (size of the ring and level of supercoiling) are enough, so as to avoid partial melting of the molecule in our simulations and consequently the local reference frame used in the continuous theoretical model is always well defined. During equilibration, the undertwisted segment of the ring is constraint so the lo-

cal twist is fixed and the simulation is run for  $10^5 \tau_{LJ}$  (simulation time). After this stage, the constraint is released at  $t = 0$  and we study the twist relaxation by monitoring its local value along the molecule. During the whole simulation, the system is confined in between two parallel planes to prevent writhe formation and in this way being able to study pure twist dynamics. We will show later that essentially the same result is obtained even without the confining walls. The exact same protocol was applied for both, the oxDNA1 and oxDNA2 models (see ESI † for details).

We run simulations at  $T = 15$  K, which allows us to study the twist dynamics in the absence of thermal fluctuations, making the protocol more efficient. As will be seen later, we recover the same behaviour from simulations at 300 K at the expenses of computation time. Such a low temperature will also, in general suppress the formation of DNA-melted-bubbles where the local twist is not defined. Furthermore, as discussed in reference<sup>10</sup>; in short, constrained and highly bent DNA, thermal fluctuations are not the main factor influencing the shape of the molecule. In addition, we prove (see Fig. S1 and Table S1) that the elastic constants are not greatly affected by this choice and therefore that the outcome from the simulations at 15 K can be compared with the theory described here. In the following, results are only discussed for simulations at 15 K unless otherwise specified.

We found that the twist evolution,  $\Omega_3(n, t)$ , for the initially undertwisted ring, can be fitted by the solution of the diffusion equation with the appropriate initial and boundary conditions (see Fig. 3 and ESI† for details). From which we extract the diffusion coefficients  $D_I^- = 0.222 \pm 0.009$  and  $D_{II}^- = 0.183 \pm 0.007 bp^2/\tau_{LJ}$  for the oxDNA1 and oxDNA2 models, respectively.

To complement this, in Fig. 4 we show results of the three local deformations for the overtwisted case. Essentially the same values of the twist diffusion coefficient were obtained,  $D_I^+ = 0.231 \pm 0.005$  and  $D_{II}^+ = 0.183 \pm 0.004 bp^2/\tau_{LJ}$ . We corroborated that simulations at  $T=300$  K show the same tendency:  $D_I^+ = 0.22 \pm 0.03$  and  $D_{II}^+ = 0.17 \pm 0.02 bp^2/\tau_{LJ}$  (see Fig. S2). Getting back to Fig. 4, we also stress here that our results are comparable to those on<sup>10</sup>. The simulations with the oxDNA2 model show that the twist-bend coupling generates the twist waves and the antiphase relation between  $\Omega_2$  and  $\Omega_3$  predicted in Eq. (4). In addition  $\lambda$  can be computed by noticing that at a fixed time (taking for example results shown by red curve in Fig. 4D), the average value over contour length of  $\Omega_3$  is shifted with respect to zero by  $1/N \sum_{n=1}^N \Omega_3(n) = 1.12^\circ/bp = 0.057$  rad/nm. This value corresponds to the factor  $\lambda/\tilde{C}$  (see Eq. (4)), from which we extract  $\lambda = 3.8 k_B T$ , in good agreement with the estimate of  $\lambda = \Delta\chi\tilde{C} = 2\pi\tilde{C}/(312 \times 0.34) = 3.4 k_B T$  from the theory. Remarkably,  $\Omega_2(n, t)$  also exhibits a diffusive behavior with basically the same diffusion coefficient as the twist diffusion:  $D_{II}^+(\Omega_2) = 0.19 \pm 0.03 bp^2/\tau_{LJ}$ . The analogous result for the undertwisted case is  $D_{II}^-(\Omega_2) = 0.20 \pm 0.04 bp^2/\tau_{LJ}$ .

All the results described above are summarized in Table 1. As we will see below, the 20% difference in the diffusion coefficient of the local twist between the two oxDNA models, along with the diffusive behavior of  $\Omega_2$ , can be explained within the theory presented in this manuscript by assuming that the dynamics of the system can be divided in three different timescales.

Temperature	$\Delta Lk$	Local deformation	Diffusion coefficient [ $bp^2/\tau_{LJ}$ ]	
			oxDNAI	oxDNAII
15 K	-1	$\Omega_3$	$0.222 \pm 0.009$	$0.183 \pm 0.007$
	+1	$\Omega_3$	$0.231 \pm 0.005$	$0.183 \pm 0.004$
	-1	$\Omega_2$	—	$0.20 \pm 0.04$
	+1	$\Omega_2$	—	$0.19 \pm 0.03$
300 K	+1	$\Omega_3$	$0.22 \pm 0.03$	$0.17 \pm 0.02$
	+1	$\Omega_2$	—	$0.19 \pm 0.03$

**Table 1** Diffusion coefficients from simulations of ring molecules (with  $N = 312$ ,  $|\Delta Lk| = 1$  and  $l = N/2$ ). Initially undertwisted ( $\Delta\chi_p = -2\pi/la$  for bp  $n \in [l, N]$ ) and overtwisted ( $\Delta\chi_p = 2\pi/la$  for bp  $n \in [l, N]$ ) rings are simulated at different temperatures (15 K and 300 K). The local deformations  $\Omega_3$  satisfies a diffusion equation for the two oxDNA models (see Figs. 3 and 4). Due to  $G > 0$ ,  $\Omega_2$  evolves diffusively only in the oxDNA2 model.

### 3.2 Dynamical equation

To discuss the dynamics, we assume that the local reference frame,  $\hat{e}_i(s, t)$  and the strain  $\Omega_i(s, t)$  are functions of both position  $s$  and time  $t$ . The dynamical equation can be derived from the compatibility relation between the strain and the angular velocity together with the force and torque balance equations<sup>17</sup>. By focusing on the twist component, the compatibility relation leads to

$$\frac{\partial \Omega_3(s, t)}{\partial t} = \frac{\partial \omega_3(s, t)}{\partial s} + \left( \hat{e}_3 \times \frac{\partial \hat{e}_3}{\partial s} \right) \cdot \frac{\partial \hat{e}_3}{\partial t}, \quad (6)$$

where  $\omega_3(s, t)$  is the rotational rate of the curve at point  $s$  at time  $t$ . The torque balance along  $\hat{e}_3$  is

$$\gamma_r \omega_3 = \Omega_1 M_2 - \Omega_2 M_1 + \frac{\partial M_3}{\partial s}, \quad (7)$$

with the rotational friction coefficient  $\gamma_r$  and the three components  $M_i = \frac{\delta \varepsilon}{\delta \Omega_i}$  of the internal torque  $\mathbf{M} = \sum_{i=1}^3 M_i \hat{e}_i$ , which are written in terms of the deviations  $\delta \Omega_i = \Omega_i - \Omega_i^0$  (see ESI †):

$$\begin{aligned} M_1 &= A_1 \delta \Omega_1, \\ M_2 &= A_2 \delta \Omega_2 + G \delta \Omega_3, \\ M_3 &= C \delta \Omega_3 + G \delta \Omega_2. \end{aligned} \quad (8)$$

For an isotropic open TWLC ( $A_1 = A_2$ ,  $G = 0$ ,  $\Omega_i^0 = 0$ ), nonlinear terms in Eq. (7) cancel out, reducing to a linear constitutive relation  $\gamma_r \omega_3 = C \partial_s (\delta \Omega_3)$ . Hence, assuming in-plane motion and deformation, Eq. (6) indicates the diffusive transport of the excess twist density  $\Omega_3(s, t)$  with the diffusion coefficient  $C/\gamma_r$ .

In our more general model, however, the story looks more complicated. In order to simplify the original nonlinear twist evolution equation (6), we have to make use of an additional argument; that there is a conserved quantity due to the topological constraint  $Lk = Tw + Wr$ . For a planar ring, the writhing number  $Wr$  is zero and the invariance of the linking number  $Lk$  implies that the total twist  $Tw = \oint ds [\chi_0 + \Omega_3(s, t)]$  is conserved. Therefore, there is a slow variable  $\delta \Omega_3(s, t)$  associated to the twist relaxation process. In fact, Eq. (6) represents the conservation of  $\Omega_3$ , where the rotation rate  $\omega_3$  is regarded as a twist current and the last term acts as a source of twist that

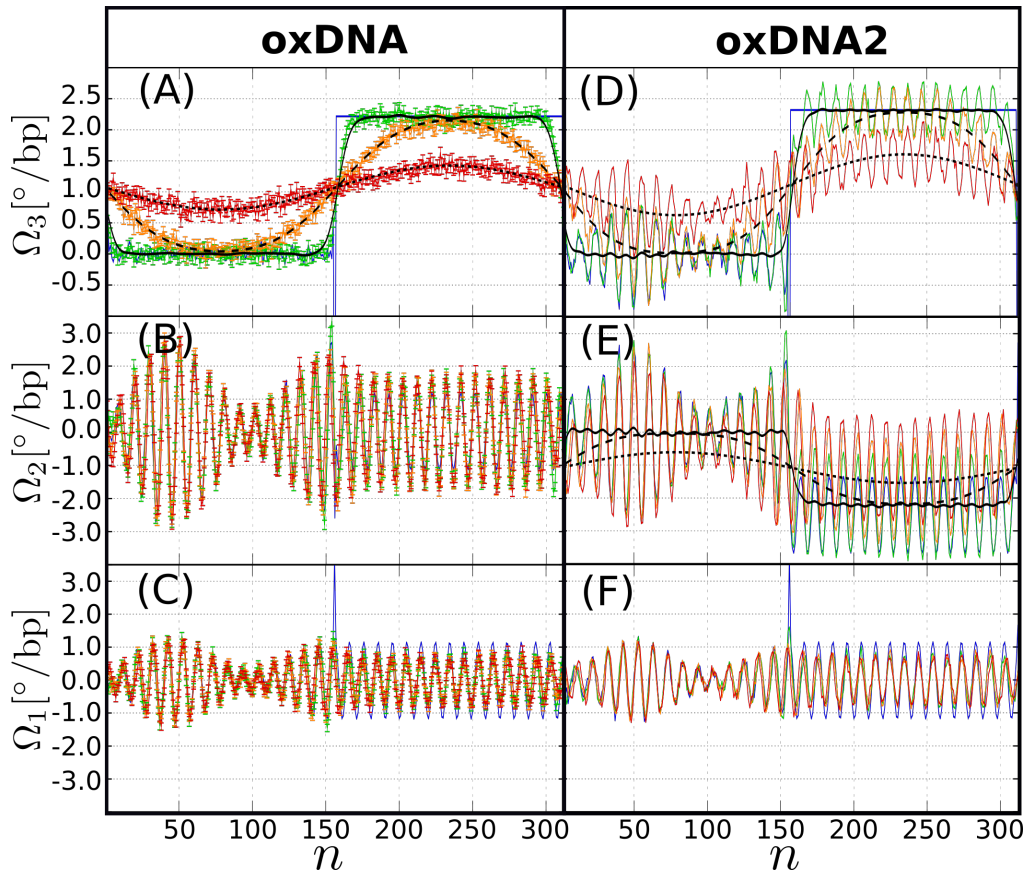


**Fig. 4** Time evolution of the local deformations from simulation (with confining planes) of the  $N = 312$  bp overtwisted ring (with  $\Delta Lk = 1$ ), captured at different timesteps: starting configuration (blue),  $50 \tau_{LJ}$  (green),  $2500 \tau_{LJ}$  (orange) and  $15000 \tau_{LJ}$  (red). Left and right panels show results for the oxDNA I and II models respectively. Color dots represent data computed from simulations and color lines are a guide for the eye. To ease the visualization, error bars are only reported for left panels. However, the size of the errorbars for right panels is similar. **(A)** and **(D)** show the average local twist deformations for the two models. As consequence of the coupling ( $G > 0$ ) the right panel displays twist waves. Solid, dashed and dotted black lines represent the fit of the data to the diffusion equation at the corresponding timesteps. This shows that twist follows a diffusive pattern. **(B)**-**(C)** are the two bending deformations  $\Omega_1$ ,  $\Omega_2$  for oxDNA1. The presence of waves with a periodicity equal to the DNA pitch is a consequence of the helical structure of DNA. Notably there are no significant changes in these variables during the twist diffusion stage, in agreement with the theory for  $G = 0$ . **(E)**-**(F)** Bending deformations for oxDNA2. The helical structure of DNA also generates waves but this time, due to the coupling between  $\Omega_2$  and  $\Omega_3$ , the overtwisted region of  $\Omega_2$  shows a clear shift consistent with Eq. (4). Furthermore,  $\Omega_2$  is also described by a diffusion equation with a very similar diffusion coefficient as  $\Omega_3$ . Solid, dashed and dotted black lines represent results from the fit performed to the data with the diffusion equation at the corresponding timesteps in panel (D). It should be also noted that the amplitude of the oscillations in  $\Omega_1$  and  $\Omega_2$  is modulated in the first half of the molecule ( $n \in [1, 156]$ ). This modulation reflects the fact that during the initial equilibration the unconstrained region displays in-plane bending deformations. For oxDNA2, due to the coupling this modulation appears also for  $\Omega_3$ .

comes from the out of plane deformations<sup>17-19</sup>. Thus, at each moment, the local bending strains  $\delta\Omega_1(s, t)$ ,  $\delta\Omega_2(s, t)$  are quickly equilibrated to the state given by  $M_1 = M_2 = 0$ , with which the twist strain  $\delta\Omega_3(s, t)$  evolves over a longer time scale. Note that the above conditions on  $M_1$ ,  $M_2$  are equivalent to finding the averages  $\langle \delta\Omega_1 \rangle$ ,  $\langle \delta\Omega_2 + G\delta\Omega_3/A_2 \rangle$  through the integration of the bending degrees of freedom ESI †, which indicates that the renormalized modulus  $\tilde{C}$  plays a role in twist dynamics. We confirm this by plugging Eq. (8) into Eq. (7) with  $M_1 = M_2 = 0$  and finding  $\gamma_r \omega_3 = \tilde{C} \partial_s (\delta\Omega_3)$ . This result, combined with Eq. (6) leads to a diffusion equation of twist

$$\frac{\partial \delta\Omega_3}{\partial t} = \tilde{D} \frac{\partial^2 \delta\Omega_3}{\partial s^2}, \quad (9)$$

with the diffusion coefficient  $\tilde{D} = \tilde{C}/\gamma_r$ . It is important to no-

tice that in order to obtain this result, we have neglected the last term in Eq. (6) since the out of plane deformations are suppressed in the confined geometry. We expect however, that this approximation is still valid for a ring without confining planes. This is because the writhing entails a global 3D rearrangement of the molecule, while the spreading of twist excess/deficit occurs locally, and therefore the former should take place in a much longer time than the latter. For this reason, the contributions of the out of plane deformations should be negligible. This argument will be confirmed later by simulations.

We predict, according to Eq. (9), that for two similar DNA molecules, one with symmetric grooves and the other with the usual asymmetry, the latter (with lower  $\tilde{C}$ ) will exhibit a slower twist diffusion. From the elastic parameters obtained in reference<sup>12</sup> and reported in ESI †, we compute the rescaled twist mod-

ulus  $\beta\tilde{C}_I = 77$  nm and  $\beta\tilde{C}_{II} \simeq 61$  nm for oxDNA1 and oxDNA2, respectively. Remarkably, the ratio between these two quantities ( $\tilde{C}_{II}/\tilde{C}_I = 0.79$ ) is in excellent agreement with the ratio of the twist diffusion coefficients found in our simulations ( $D_{II}/D_I = 0.81 \pm 0.02$ ), obtained by averaging the results from over and undertwisted rings.

Moreover, our argument ( $M_2 = 0$ ) suggests that the twist diffusion in DNA is accompanied by a *bend diffusion* that is induced by the twist-bend coupling. Figure 4(E) demonstrates that this is indeed the case for oxDNA2, where  $\Omega_2$  relaxes diffusively following the behavior of  $\Omega_3$  with basically the same diffusion coefficient. Such a phenomenon is not observed in the oxDNA1 without groove asymmetry.

We also note that since the diffusion coefficient in Eq. (9) only depends on the elastic parameters and does not depend explicitly on the temperature of the system, we expect a similar behavior at room temperature (see Fig. S2), the temperature though, affects the persistence lengths  $l_\tau$  and  $l_b$ .

It is relevant to recall here that although the role of DNA sequence on the twist diffusion is beyond the scope of this manuscript, we expect some reasonable behavior within the limitations of our model. Currently, the molecule in our simulations is made of only GC pairs; changing the sequence of the system (so the molecule is no longer a homopolymer), will introduce a  $s$ -dependence on the elastic parameters that is not considered in our theory. However, for DNA repeated sequences an effective value of the elastic parameters can be computed in the oxDNA models (see Fig. S4 and Table S2 of reference<sup>12</sup>). As expected, these values show that decreasing the GC content will in general soften the elastic response of the DNA. Provided that the system does not show strong structural changes (like local melting) this would imply that the diffusion coefficient would also decrease. In table S2 we compute the renormalized twist modulus using the values of the elastic constants on reference<sup>12</sup> for different sequences. We found that the ratio  $\tilde{C}_{II}/\tilde{C}_I$  does not seem to change with the sequence in the oxDNA models. An additional interesting observation is that for any of the two models, the value of  $\tilde{C}$  and therefore of  $\tilde{D}$ , can change for a factor up to 12.5% for the sequences analyzed (compare for example, polyCG and polyAT results). This striking difference indicates the relevance of sequence in the DNA dynamics, and confirms the need of theoretical models that account for the sequence-dependent DNA elasticity. This could be a key aspect in the understanding of, for example, nucleosome dynamics<sup>20</sup>.

It is important to state that the theory introduced in this manuscript is appropriate to describe systems without strong deformations, such as, melted bubbles or highly bend sections of DNA. These considerations become relevant in the study of DNA mini-circles ( $L < l_b$ ) and thus, it requires the introduction of a more general theory<sup>21,22</sup>.

### 3.3 Buckling instability

We investigate the dynamics of the same system without confining planes. Figure 5 shows the time evolution of the total twist ( $\text{Tw}$ ), where we observe that at short times (smaller than  $10^5 \tau_{LJ}$ ) the

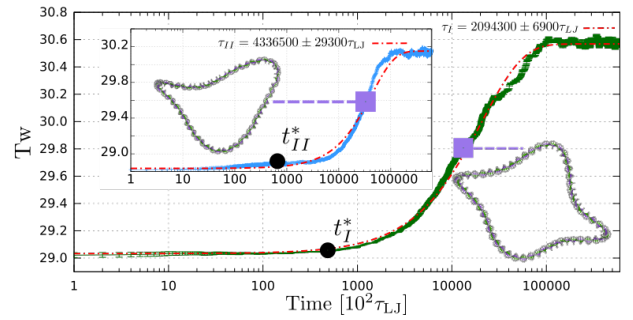


**Fig. 5** Time evolution of  $\text{Tw}$  for undertwisted oxDNA1 (main) and oxDNA2 (inset). Red dashed lines represent an exponential fit to the data  $\text{Tw}(t) = c1 - c2 * \exp(-t/\tau)$ . The value of  $\tau$  obtained from the fit to the oxDNA1 and oxDNA2 models are  $2.09 \times 10^6 \tau_{LJ}$ ,  $4.33 \times 10^6 \tau_{LJ}$ . Purple squares show the timestep at which the buckling of the system (shown in the snapshots) takes place. The diffusion time,  $t^*$ , is depicted with a black dot.

change in  $\text{Tw}$  is insignificant and in consequence that the out of plane deformations of the ring are negligible. Furthermore, the time required for the deficit of twist to diffuse across the entire ring, a distance of  $N - l$  ( $= N/2$ ) bp, is given by  $t^* \approx (N - l)^2 / 2\tilde{D}$ . Since the value of  $t^*$  is  $t_I^* = 5.53 \times 10^4$  and  $t_{II}^* = 6.76 \times 10^4 \tau_{LJ}$  for the oxDNA1 and oxDNA2 models (both smaller than  $10^5 \tau_{LJ}$ ), respectively, our assumption of neglecting the last term in Eq. (6) during the diffusion stage seems to be appropriate even after getting rid of the confining planes.

At  $t \sim t^*$ , i.e. at the end of stage  $II$ , we verified that the  $s$ -dependence of the  $\Omega_i$ 's, displays the features (i-iii) predicted in Eq. (4) (see ESI† and Movies S1-S2). As the simulation continues ( $t > t^*$ ), the magnitude of the shift in  $\Omega_3$  (and also in  $\Omega_2$  for oxDNA2 due to nonzero  $G$ , see Eq. (4)) decreases approaching to zero and the interchange between twist and writhe takes place. This is indicated by the rapid increase of  $\text{Tw}$  shown in Fig. 5. The buckling of the molecule is reflected in the large scale ( $\gg 2\pi/\chi_0$ ) bending deformations (see supplementary movies). The number of local minima (maxima) found in the envelope of the bending deformations, referred as the bending mode number  $m$ , quantifies the number of times that the ring bends back and forth across its contour length. In Fig. S6 we show the value of  $m$  computed from simulations as a function of time. It should be noted here that since the local twist relaxation exhibits a diffusive behaviour, we observed in our simulations (for example when comparing  $N = 624$  bp,  $l = 312$  bp with different  $\Delta Lk$ , either -1 or -2) that the diffusion coefficient is not affected by the level of supercoiling. As expected also, the time of diffusion  $t^*$  is the same in both cases. However, due to mechanical stress, the initial writhing takes less time for the case with higher level of supercoiling.

From the discussion so far, one may expect that the behavior of the DNA model can be mapped to that of an isotropic TWLC using the renormalized moduli  $\tilde{A}$  and  $\tilde{C}$ . We now show that when describing the buckling of DNA, this naive expectation only holds in a qualitative level, but fails to explain the quantitative aspects. The linear stability analysis for the isotropic TWLC ring predicts that the most unstable mode ( $m^*$ ) depends on the ratio of the twist and bend elastic moduli  $C/A$  and the excess linking number

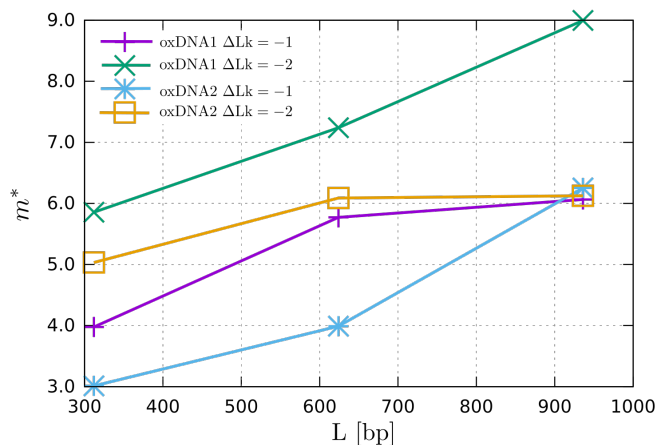


**Fig. 6** Bending mode ( $m^*$ ) selected by the system as function of the total length of the ring.

$\Delta Lk$  such that the smaller the ratio  $C/A$ , the smaller the selected mode number  $m^*$  at a fixed  $\Delta Lk$  (see Fig. S5)<sup>23</sup>. This mode will grow faster than the others, and therefore will be the first observed at the onset of the buckling.

We show in Fig. 6 the most unstable mode  $m^*$  obtained from simulations as function of the DNA size. For an  $N = 312$  bp ring with  $\Delta Lk = -1$ , we find  $m^* \simeq 4$  for oxDNA1 and  $m^* \simeq 3$  for oxDNA2 (see snapshots in Fig. 5). Although these results are in good agreement with the mapping mentioned above (see ESI†), this should not be regarded as a complete success. Remarkably, we numerically find that  $m^*$  depends on the ring length, a feature absent in the linear theory of isotropic TWLC. On the other hand, our results also suggest a satisfactory agreement in a more qualitative level; the ratio  $\tilde{C}/\tilde{A}$  of oxDNA2 (1.6) is smaller than the one for oxDNA1 (2.1), and as expected, so is the observed  $m^*$ .

The main reason for the discrepancy may lie in the helical nature of DNA (intrinsic twist  $\chi_0$ ) and anisotropic bending. For a ring made from isotropic and untwisted filament,  $A_1 = A_2$  and  $\chi_0 = 0$ , the configuration that minimizes the bending energy is the one of a planar circle with constant curvature. However, non-zero  $\chi_0$  leads to the periodic variation of bending strain  $\Omega_1(s)$  and  $\Omega_2(s)$  along the contour. In DNA, coupled with this is the bend anisotropy, which results in preferential bending along the soft axis. As a result, a slightly off-planar configurations with varying curvature are explored in order to minimize the bending energy<sup>11</sup>. These inhomogeneity may likely provide a “hot spot” for the buckling instability. The possibility of incommensurate periodicity between the unstable mode and the underlying bending oscillation may further complicate the situation. The amplitude of the bending oscillation tends to decrease with ring size (Eq. 4), but at the same time, the effect of thermal fluctuation becomes more relevant, which tends to smooth the transition.

## 4 Conclusions

Through a careful numerical and theoretical analysis, we have identified three distinctive time scales in the relaxation dynamics after a local twist perturbation introduced in a torsionally constrained DNA ring. (*I*) In the fastest scale, the local bending re-

laxation takes place given the twist strain at that moment. (*II*) The twist diffusive relaxation proceeds more slowly governed by the conservation law with a topological origin. (*III*) After the completion of twist diffusion, the remanent twist stress, if sufficiently strong, makes the whole ring undergo a buckling transition in a much longer time scale. It is this time scale separation that allows us to reduce the original nonlinear time evolution equation to the simple diffusion equation in the twist relaxation process (*II*). It also provides rich physical insights on how the molecular features of DNA, and in particular the groove asymmetry, plays a role in the twist dynamics. Here, we have shown that the twist diffusion coefficient is entirely determined by the renormalized twist modulus  $\tilde{C}$ , which is smaller than the bare modulus  $C$ , due to the twist-bend coupling induced by the groove asymmetry. One remarkable consequence of  $G > 0$  is that one component of bend ( $\Omega_2$ ) exhibits the concomitant diffusive relaxation, which is tightly coupled with the twist diffusion.

Although recent works on statics<sup>13</sup> suggest that the more realistic model reflecting molecular details of the DNA double-helix can be mapped to a simple isotropic TWLC by using the renormalized bending and twisting moduli  $\tilde{A}$ ,  $\tilde{C}$ , and our present results suggest its applicability also to dynamics, we have shown that such a mapping is not almighty. A concrete counter-example is the twist-buckling, for which the instability mode can be predicted only qualitatively, but not quantitatively.

Hydrodynamic effects are neglected in the oxDNA model and hence, one needs to be cautious in interpreting the units obtained from simulations. Keeping this point in mind, it is still useful to provide a rough time scale estimation in real experiments. With  $\tau_{LJ} = 1.7$  ps (see ESI†), the diffusion of twist across the entire contour length of a  $1 \mu\text{m} \sim 3000$  bp long DNA-molecule would take a time  $t^* \sim 0.1$  ms. If this molecule is over/under twisted by 10 helical turns in such a way that the level of supercoiling is  $\sigma = \Delta Lk/Lk_0 \sim 0.033$ , a rough estimate of the writhing time could be given by observing that the plateau in Fig.5 is reached after a time ( $\sim 200 t^*$ ) that is two orders of magnitude larger than  $t^*$ . In our example of the  $1 \mu\text{m}$  molecule this represents 20 ms. Continuing with this approximation, we would expect that a plectoneme is formed in a similar time (that scales with the length of the molecule) in a torque-response experiment at low force ( $f < 1$  pN) and high salt concentration (to avoid melted-bubble formation), such as the one reported in<sup>24</sup>. Therefore, the time evolution of the end-to-end distance, after quickly adding enough helical turns to obtain  $\sigma = 0.03$ , would reach a plateau in about the same time-scale.

Finally, there is recent evidence<sup>9</sup> that the local twist of the DNA-nucleosome complex in equilibrium, that was extracted from X-ray crystallography experiments, resembles the local twist obtained for DNA minicircles with twist-bend coupling. Closely related to this result, is that local bending-modulations are observed in DNA minicircles with over/under twisting<sup>10</sup>. These modulations lead to a change of the local curvature (reflected in the change of shape from the minicircle to a polygon) that may influence the way that twist defects propagate along the nucleosome and therefore would be important in the nucleosome-slide mechanism. Complementing this picture, here we consider one

more aspect that might be relevant in the dynamics of the system. A local twist perturbation, produced for example by the transcription of DNA in a distant site to the DNA-nucleosome complex, could quickly diffuse, reach the complex and disrupting it; an interesting feature to be considered for subsequent work. Therefore, the twist-bend coupling should be recognized as a key aspect in order to capture a clearer picture of the dynamics of this system.

### Conflicts of interest

There are no conflicts to declare.

### Acknowledgements

This work was supported by JSPS KAKENHI (No. JP18H05529) from MEXT, Japan, and JST, PRESTO (JPMJPR16N5).

### References

- 1 C. A. Brackley, S. Taylor, A. Papantonis, P. R. Cook and D. Marenduzzo, *PNAS*, 2013, **110**, E3605–E3611.
- 2 B. Alberts, A. Johnson, L. Julian, M. Raff, K. Roberts and P. Walter, *Molecular Biology of the Cell. 4th edition*, New York: Garland Science, 2002.
- 3 P. R. Cook and D. Marenduzzo, *Journal of Cell Biology*, 2009, **186**, 825–834.
- 4 L. F. Liu and J. C. Wang, *PNAS*, 1987, **84**, 7024–7027.
- 5 L. Baranello, D. Levens, A. Gupta and F. Kouzine, *BBA - Gene Regulatory Mechanisms*, 2012, **1819**, 632 – 638.
- 6 C. A. Brackley, J. Johnson, A. Bentivoglio, S. Corless, N. Gilbert, G. Gonnella and D. Marenduzzo, *Phys. Rev. Lett.*, 2016, **117**, 018101.
- 7 F. Kouzine, A. Gupta, L. Baranello, D. Wojtowicz, K. Ben-Aissa, J. Liu, T. M. Przytycka and D. Levens, *Nature Structural & Molecular Biology*, 2013, **20**, 396–403.
- 8 J. F. Marko and E. D. Siggia, *Macromolecules*, 1994, **27**, 981–988.
- 9 E. Skoruppa, S. K. Nomidis, J. F. Marko and E. Carlon, *Phys. Rev. Lett.*, 2018, **121**, 088101.
- 10 M. Caraglio, E. Skoruppa and E. Carlon, *The Journal of Chemical Physics*, 2019, **150**, 135101.
- 11 D. Norouzi, F. Mohammad-Rafiee and R. Golestanian, *Phys. Rev. Lett.*, 2008, **101**, 168103.
- 12 E. Skoruppa, M. Laleman, S. K. Nomidis and E. Carlon, *The Journal of Chemical Physics*, 2017, **146**, 214902.
- 13 S. K. Nomidis, F. Kriegel, W. Vanderlinden, J. Lipfert and E. Carlon, *Phys. Rev. Lett.*, 2017, **118**, 217801.
- 14 T. E. Ouldridge, A. A. Louis and J. P. K. Doye, *Phys. Rev. Lett.*, 2010, **104**, 178101.
- 15 T. Ouldridge, A. Louis and J. Doye, *J. Chem. Phys.*, 2011, **134**, 085101.
- 16 Y. A. G. Fosado, D. Michieletto, C. A. Brackley and D. Marenduzzo, *arXiv 1906.03287*.
- 17 T. R. Powers, *Rev. Mod. Phys.*, 2010, **82**, 1607–1631.
- 18 R. D. Kamien, *Eur. Phys. J. B*, 1998, **1**, 1–4.
- 19 H. Wada, *Physical Review E*, 2011, **84**, 042901.
- 20 B. Eslami-Mossallam, H. Schiessel and J. van Noort, *Advances in Colloid and Interface Science*, 2016, **232**, 101 – 113.
- 21 J. Yan and J. F. Marko, *Phys. Rev. Lett.*, 2004, **93**, 108108.
- 22 F. LankaÅa, R. Lavery and J. H. Maddocks, *Structure*, 2006, **14**, 1527 – 1534.
- 23 F. Tanaka and H. Takahashi, *The Journal of Chemical Physics*, 1985, **83**, 6017–6026.
- 24 K. Yoshida, D. Ando, M. Makuta and Y. Murayama, *Journal of the Physical Society of Japan*, 2018, **87**, 093801.

Diffusion

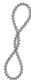
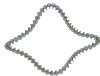
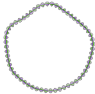
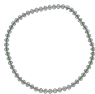
Buckling

Writhing

Page 9 of 9

Soft Matter

Symmetric  
grooves  
( $G=0$ )



Asymmetric  
grooves  
( $G>0$ )

